Available online at www.sciencedirect.com

ScienceDirect

Advances in Space Research xxx (2019) xxx–xxx

ADVANCES IN SPACE RESEARCH (a COSPAR publication)

www.elsevier.com/locate/asr

Composite analysis of North Atlantic extra-tropical cyclone waves from satellite altimetry observations

S. Ponce de León *, J.H. Bettencourt

Centre for Marine Technology and Ocean Engineering, Instituto Superior Técnico, Lisboa, Portugal

Received 24 February 2019; received in revised form 13 July 2019; accepted 16 July 2019

Abstract

The north Atlantic Ocean is regularly traversed by extratropical cyclones and winter low pressure systems originated in the Western part of the basin that can potentially generate dangerous extreme sea states. In this paper we study the significant wave height distribution of extratropical cyclones using merged satellite altimetry data to produce composite maps of this sea state variable. Although there are large variations among individual cyclones, the compositing method allows obtaining general features. We find that the higher waves are in the south-eastern quadrant of the cyclone, due to the extended fetch mechanism. The highest wave heights are found during the 48 h period when the cyclone's strength is maximum. The strongest cyclones have higher waves over most of the eastern half, due to their northward propagation tendency.

Keywords: Extra-tropical cyclones; Satellite altimetry; Significant wave height; Wind waves; North Atlantic; Storm tracks

1. Introduction

Extra-tropical cyclones (cyclones hereafter) are synoptic scale features of the mid latitudes that have a basin-wide impact on the weather and climate of the North Atlantic. During their passage, strong winds, precipitation and temperature changes are frequently recorded (Hewson and Neu, 2015; Ulbrich et al., 2009) and are important in transmitting the effects of low-frequency climate variability to the environment and society (Graham and Diaz, 2001). Moreover, cyclones help to determine low-frequency variability in the midlatitude circulation (Trenberth and Hurrell, 1994) and contribute to the subtropical to higher latitude heat and moisture transport and to the air-sea exchange of heat and momentum (Hurrell and van Loon, 1997). North Atlantic cyclones have also a strong effect on the mean sea state (Wang and Swail, 2002) and in an extreme events (Bell et al., 2017; Breivik et al., 2014; Ponce de León et al., 2015). Indeed, in the North Atlantic, very high waves are to be found in the storm track region of the basin (Takbash et al., 2018; Young, 1999) and the west coast of Europe is regularly exposed to huge swells generated by the North Atlantic cyclones that cross the basin from west to east, with significant socio-economic consequences and increased coastal vulnerability (Lozano et al., 2004; Pinto et al., 2014).

Cyclone structure and evolution have been studied extensively and reviews of this subject can be found in Hewson and Neu (2015) and Semple (2006). Cyclones that affect Western Europe are mainly formed in the western North Atlantic as weak atmospheric frontal waves that interact with upper level drivers such as throughs or strong jets, with ensuing cyclogenesis (Hewson, 2009), favored by latent heat release. During the cyclone evolution,

* Corresponding author at: Pavilhão Central, Instituto Superior Técnico, Av. Rovisco Pais, 1, 1900-001 Lisboa, Portugal.

E-mail address: soniaponcedeleon@tecnico.ulisboa.pt (S. Ponce de León).

https://doi.org/10.1016/j.asr.2019.07.021

0273-1177/

characteristic airflows, defined by their position with respect to the cyclone's center (Fig. 1), will occur: the warm conveyor belt (WCB) that moves heat, moisture and momentum poleward ahead of the cold front; the cold conveyor belt (CCB), composed of cold air to the northeast of the cyclone that develops ahead of the warm front and moves westward; the "sting jet" which is a small region with exceptionally high surface winds that occurs near the tip of the bent back front. Given the individual variability of cyclones, not all three airflows occur always, or occur with the same intensity. However it has been found that each is capable of influencing the ocean wind wave field of cyclones (Bell et al., 2017; Kita et al., 2018).

The effect of individual cyclones on North Atlantic ocean wind waves has been studied previously. Ponce de León and Guedes Soares (2014) studied the distribution of extreme wave parameters under two cyclones of February 2007 and found that these parameters are higher in the fourth quadrant, between 90° and 180° measured clockwise from the cyclone's direction and when the wind and wave propagation directions are aligned; Bell et al. (2017) studied the relationship between storms and extreme waves in the North Sea and found that the extreme waves in the central North Sea were caused by WCB and CCB winds; Kita et al. (2018) studied a January 2013 cyclone in the Northwestern Pacific and found that both the warm and cold zones of the cyclone, at either side of the warm front, had narrow directional and frequency spectra.

However, the individuality of each cyclone makes it difficult to extract general information about the average sea state of North Atlantic cyclones from specific cases (Ponce de León and Guedes Soares, 2015).

Cyclone compositing, using large reanalysis datasets and cyclone tracking algorithms(Gramcianinov et al., 2019; Ulbrich et al., 2009), provides more generality than individual cyclone case studies by averaging cyclone structure (Dacre and Gray, 2009). Among others, compositing was used to study explosive cyclogenesis (Sanders and Gyakum, 1980), precipitation fields (Chang and Song, 2006), cloud structure (Field and Wood, 2007) and air-sea turbulent fluxes (Rudeva and Gulev, 2010). A composite analysis of wave fields in NW Pacific cyclones was carried out in Kita et al. (2018), using a hindcast wave simulation.

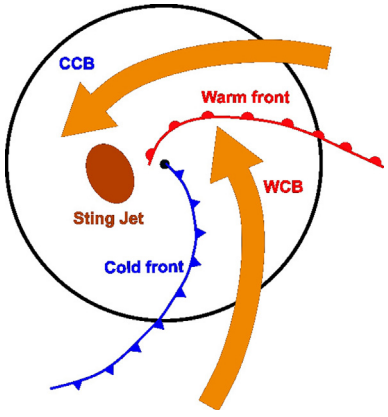

Fig. 1. Diagram of characteristic airflows in an idealized extra-tropical cyclone WCB (Warm conveyor belt), CCB (Cold conveyor belt).

Nowadays, large cross-calibrated multimission databases of surface wind and Hs from altimetry are available to study ocean wind, wave properties and climate (Young and Donelan, 2018). Although satellite altimetry suffers from incomplete temporal and spatial coverage, the amount of available data from successive satellite passes enables the calculation of wind and Hs distributions and allows estimating climatological fields, trends and extreme values prediction (Alves and Young, 2003; Izaguirre et al., 2011).

In view of the risks associated with extra-tropical storms and the severe sea states associated with them, in this paper we use a large multimission satellite altimeter wind and Hs database and a database of Northern Hemisphere extra-tropical cyclones to construct composites of cyclone Hs and study the structure of the average Hs distribution and its variations with life cycle and cyclone intensity. The paper is structured as follows: in Section 2 we describe the data sources and the compositing method, Section 3 details our results and Section 4 is dedicated to the discussion and conclusions of our study.

2. Data and methods

2.1. Database of extra-tropical cyclones

The cyclone database consists of a 58-year (1958 to 2016) record of daily cyclone characteristics for the Northern Hemisphere (Serreze, 2009). The cyclone data is obtained by the Serreze et al. (1997) algorithm from the daily sea-level pressure (SLP) fields of the NCEP/NCAR Reanalysis. The data is provided at 6-hour intervals at a spatial resolution of 250 km.

2.2. The GLOBWAVE altimetry database

The GLOBWAVE dataset (http://globwave.ifremer.fr/) is a uniform, harmonized, quality controlled, multi-sensor set of satellite wave data and ancillary information in a common format, with a consistent characterization of errors and biases. The data used in this study is the altimeter multi-mission Hs which is a merged global altimeter Hs data set (Version 4, October 2008) from six altimeter missions: ERS-1 and ERS-2, TOPEX/Poseidon, GEOSAT Follow On (GFO), Jason-1 and ENVISAT (produced by CERSAT/IFREMER).

The quality of altimeter derived significant wave heights (Hs) has been extensively verified (Abdalla et al., 2010; Janssen et al., 2007; Queffelou, 2004; Zieger et al., 2009). The altimeter estimates Hs from the slope of the leading edge of the radar return. The accuracy of the altimeter measurements depends on several sources: instrument noise, atmospheric errors, sea-state bias and errors in orbit

Please cite this article as: S. Ponce de León and J. H. Bettencourt, Composite analysis of North Atlantic extra-tropical cyclone waves from satellite altimetry observations, Advances in Space Research, https://doi.org/10.1016/j.asr.2019.07.021

determination. Each source contributes with errors of the order of centimeters (Martin, 2014; Young et al, 2017). The GLOBWAVE altimeter Hs error analysis was carried out using a quality-controlled dataset of collocations with *in situ* buoys (Ash et al., 2010). Hs standard error for the satellite missions varied between 0.08 m and 0.146 m for Hs < 1 m, between 0.253 m and 0.317 m for Hs = 4 m and between 0.47 m and 0.698 m for Hs = 8 m.

The altimeter can also measure wind speed U10, although less accurately than the wave height. The wind speed is obtained from the backscatter radar cross-section using empirically determined relationships based on buoy data comparisons, with reported root mean square errors below 1.7 ms^{-1} for several cross-calibrated altimeters (Zieger et al., 2009).

2.3. Mapping methodology

The procedure to map the Hs around the cyclone centre is composed by the following steps:

(1) Selection of the cyclones
(2) Identification of the satellite tracks that cross the cyclone area
(3) Download of the satellite data identified in step 2.
(4) Mapping of the satellite data to a polar grid centred on the cyclone's centre

Due to practical reasons the mapping is done year by year. For each year, a composite Hs field is obtained by averaging the individual cyclone Hs maps. A further average is performed afterwards to obtain the 15-year composite map of Hs.

2.3.1. Selection of the cyclones

The selection of the cyclones that enter the census is made according to the following criteria:

a) The cyclogenesis occurs between longitudes 90°W and 10°W
b) The cyclone center does not move northward of latitude 70°N
c) The track extends over at least 15° of longitude
d) The cyclone lasts more than 3 days
e) The cyclone isn't stationary
f) The cyclone intensifies at least 2 hPa of SLP during its lifetime

Criteria a) and b) were used to select those cyclones that have their genesis in the western part of the NA basin, as this is the generation region of most strong cyclones that affect Europe (Hewson and Neu, 2015) and to limit the region of influence of the cyclone to the subpolar NA basin. Criteria c) and d) have the purpose of selecting cyclones that due to their longevity and track length have an impact on the associated ocean wave field. Criterion e) tries to avoid cyclones that have a stationary period in their lifetimes and criterion d) is used to select cyclones that intensify during their lifetime.

2.3.2. Identification of the satellite tracks

After selecting the cyclones, we have the time series of their center positions $c(t)$. By defining a constant cyclone radius R, we define for each time t a square region of side length $2R$ centered at $c(t)$ and whose sides are distanced R km to the west and east and to the north and south of $c(t)$ (Fig. 2). We then use the scripting facilities to query the GLOBWAVE database for the track files that cross the square between 3 h before and 3 h after the corresponding t. This query is performed for each satellite product in the GLOBWAVE database.

2.3.3. Mapping of the Hs data

To map the Hs to the cyclone area we employ a polar coordinate system (Fig. 3) that uses the distance r to the center and the azimuth α of the Hs measurement with respect to the meridian that crosses the center location c, so that $\alpha = 0°$ corresponds to a measurement located north of c and $\alpha = 90°$ corresponds to a measurement east of c. To create a map of Hs around the cyclone center, the circle of radius R centered at c is divided in segments bounded by N_i radial distances to c and N_j azimuths (Fig. 3, shaded area). At each t, the Hs of each segment is computed as the average of the valid altimeter measurements that fall inside the segment.

For the fixed cyclone radius, we used $R = 500$ km following the analysis of Schneidereit et al. (2010), that fitted a Gaussian function to the 1000 hPa geopotential height to located cyclone centers in the ERA-40 data in the Northern Hemisphere and found cyclone radius that varied between 300 and 500 km, showing weak growth during the cyclone's life cycles. Kita et al. (2018) used a 5° elliptical area around the cyclone's center that, at the latitude of the region analyzed, gives major and minor axis of 554 km and 482 km, respectively.

We used $N_i = N_j = 10$, so that each segment has a fixed radial length of 50 km and is 36° wide. These values were chosen as a compromise between the speed of execution of the procedure and the need to obtain a map that represents well enough the variation of Hs around the cyclone, since very large segments would average out the variations in the Hs measurements. Smaller segments, on the other hand, would cause longer execution times and more cases of segments without measurements. Indeed, even with the chosen values, not all segments have tracks that cross them and thus the map of the cyclone Hs is only partially filled each time. Due to this lack of coverage it is not possible to define an average Hs map for each cyclone, as was the case for Kita et al. (2018), but given enough cyclones it is possible to compute an average Hs for each segment and to obtain an average Hs distribution in the cyclone. In our mapping procedure the number of observations in each grid cell (Fig. 4) varies between ~1000 in the inner radii and ~20,000 in the outer radii (Fig. 4), but the observation

Please cite this article as: S. Ponce de León and J. H. Bettencourt, Composite analysis of North Atlantic extra-tropical cyclone waves from satellite altimetry observations, Advances in Space Research, https://doi.org/10.1016/j.asr.2019.07.021

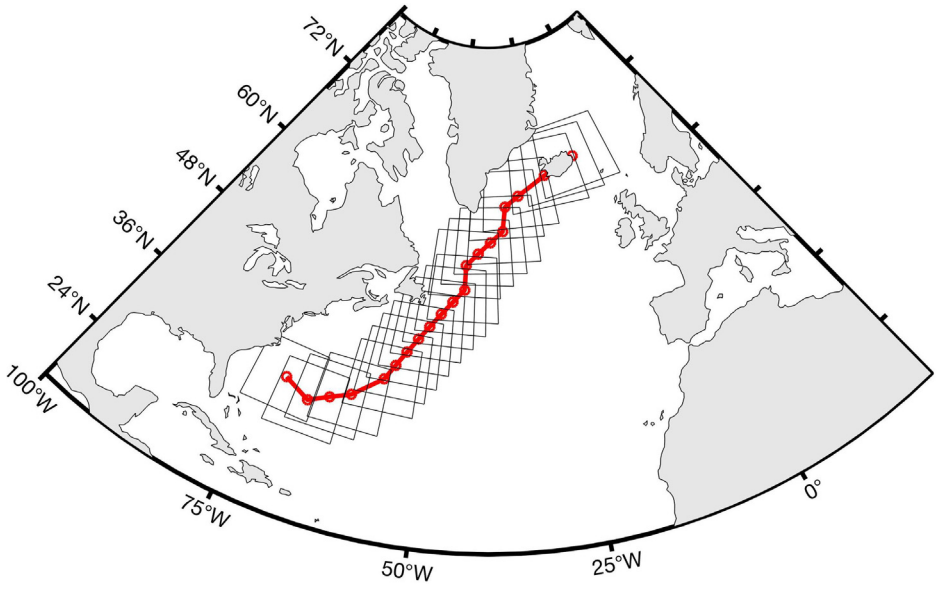

Fig. 2. Trajectory of ETC #7 of 2009 (red line) with center positions (red open circles) and the cyclone centred squares used to identify altimeter tracks that cross the cyclone path. The cyclone was tracked from 16/2/2009 12UTC to 21/2/2009 18UTC. (For interpretation of the references to colour in this figure legend, the reader is referred to the web version of this article.)

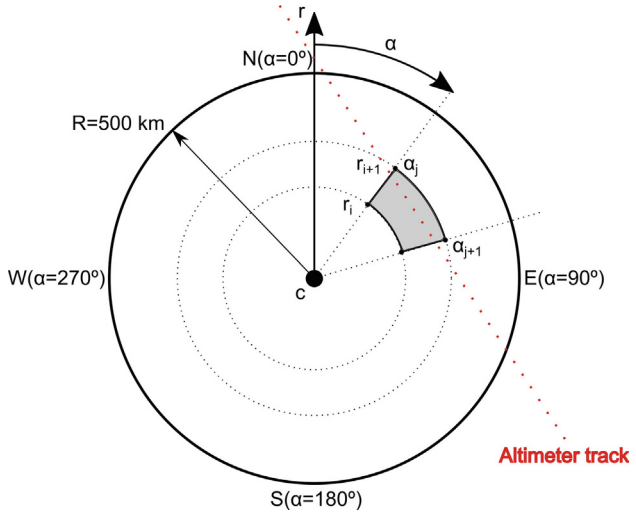

Fig. 3. The cyclone centred coordinate system used in the mapping procedure. Dotted line represents an altimeter track. The Hs of the segment (shaded area) is the average of the Hs altimeter measurements that fall inside the segment.

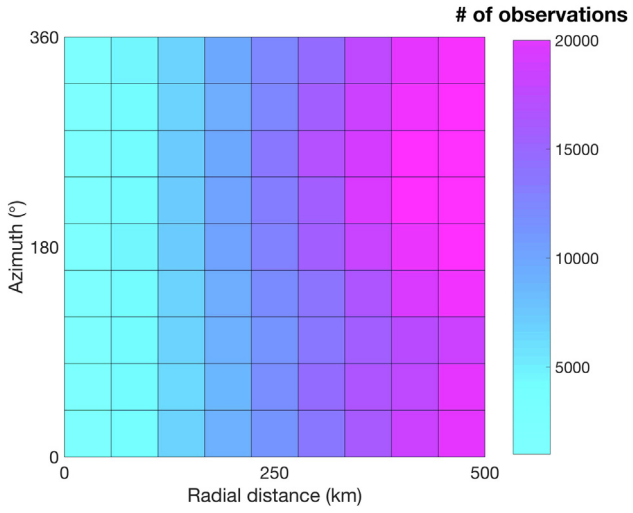

Fig. 4. Number of altimeter observations in each grid cell. Radial distance is from the cyclone center and azimuth is measured clockwise from North.

density, i.e. the number of observations per unit area is basically constant and close to 1 observation/m^2.

Since the composite maps obtained are somewhat coarse, they are smoothed by subdividing each segment in 25 smaller segments and interpolating the map data at each subdivision.

3. Results

We analyzed a 15-year period from 1998 to 2012, resulting in a cyclone census with 742 cyclones. On average, 50 cyclones were selected per year. The year with the highest number of cyclones was 2002 (59) and the year with the lowest number of cyclones was 2012 (43). For the 15-year period, 22,008 altimeter track files were processed.

The cyclones are mainly generated in the Gulf Stream region of the US east coast (Fig. 5a), that is one of the major storm formation areas, where the local sea surface temperature gradients are a precondition to cyclone generation and intensification (Giordani and Caniaux, 2001; Hoskins and Valdes, 1989). The cyclone trajectories (Fig. 5b) follow the well-known North Atlantic storm track region (Ulbrich et al., 2009).

Cyclones with lifetimes larger than 3.5 days account for 73% of the total cyclone count (Fig. 5c). These cyclones decay in the Labrador and Baffin Bay (LB) region, the

Please cite this article as: S. Ponce de León and J. H. Bettencourt, Composite analysis of North Atlantic extra-tropical cyclone waves from satellite altimetry observations, Advances in Space Research, https://doi.org/10.1016/j.asr.2019.07.021

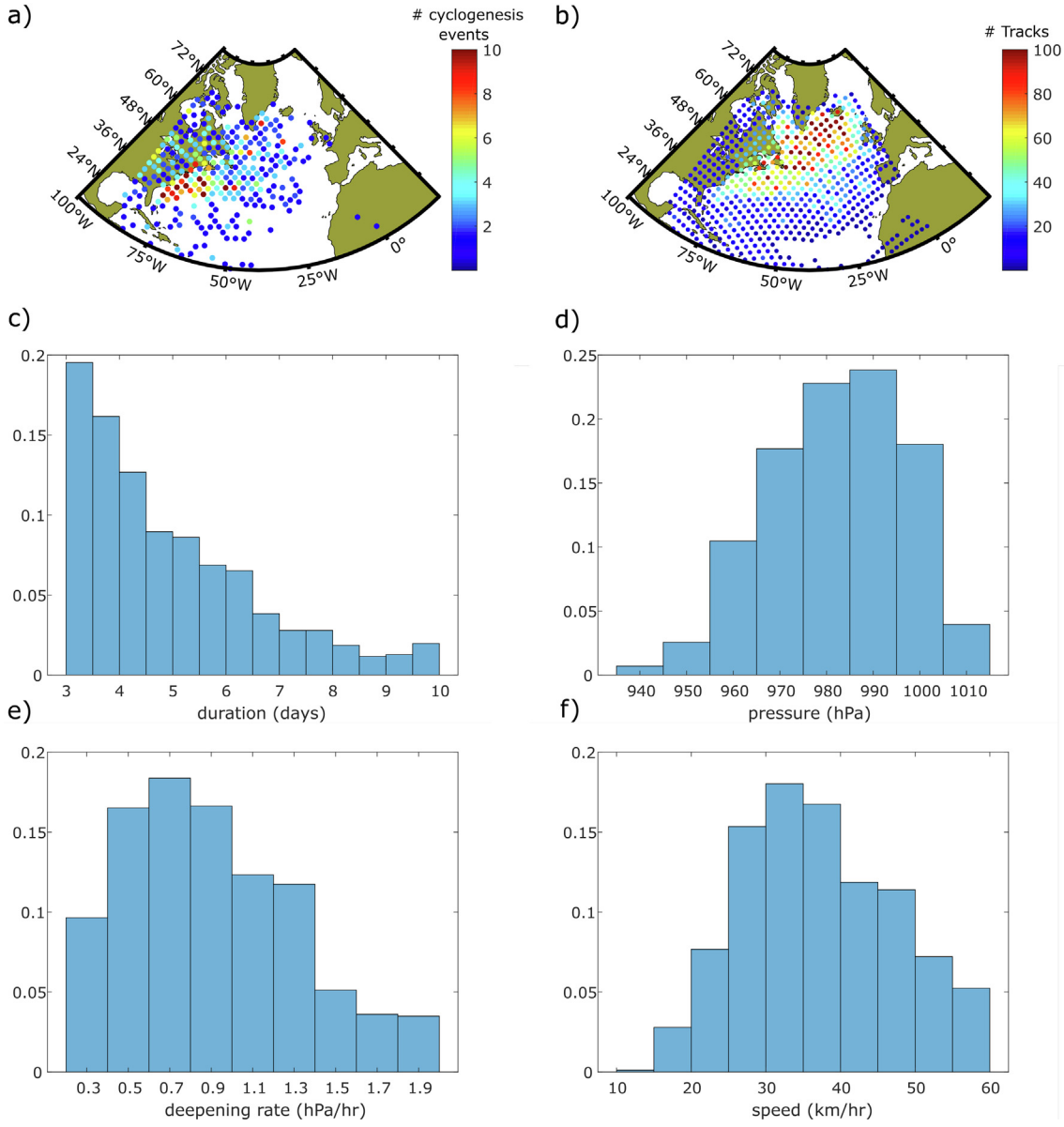

Fig. 5. Cyclone characteristics. (a) Map of cyclogenesis location. (b) Map of cyclone tracks. (c) Histogram of cyclone lifetimes. (d) Histogram of sea level pressure minimum. (e) Histogram of deepening rate. (f) Histogram of cyclone mean propagation speed.

Norwegian and Greenland Seas (NG) region, the Mid Atlantic (MD) region and the Iberia – Biscay (IB) region (Rudeva and Gulev 2010, Fig. 12a). The cyclones decaying in LB and NG are the most intense, faster deepening and propagate faster while the IB cyclones are weaker, slowly deepening and slowly moving but are longer-lived (Rudeva and Gulev, 2010).

Cyclones with center pressure below 960 hPa (Fig. 5d) account for 8% of the total cyclone count, a substantially lower value than the 14% of Northern Hemisphere (NH) cyclones that have minimum SLP below this level in the census of Rudeva and Gulev (2010). This may be due to the inclusion of longer lived but weaker cyclones in our census. The fastest deepening cyclones (maximum deepening rate >1 Bergeron or 24 hPa/24 h, Fig. 5e) are 38% in our census, while in the NH census these cyclones account for 20% of total cyclone count. This higher fraction of rapidly intensifying cyclones in our census could be due to the higher percentage of cyclones generated in the Gulf Stream region, that shows a shorter intensification period (Dacre and Gray, 2009). The census of Rudeva and Gulev (2010) of Gulf Stream generated cyclones had a 58% fraction of rapidly intensifying cyclones, which supports this explanation. Cyclones propagating slower than 30 km/h (Fig. 5f) account for 26% of the census (24% for the NH census).

3.1. Wind speed and significant wave height composites

The altimeter 10-m wind speed 15-year composite (Fig. 6a) has maximum values of ~12 m/s located in the 4th quadrant (Southeast). This agrees with the analysis of

Please cite this article as: S. Ponce de León and J. H. Bettencourt, Composite analysis of North Atlantic extra-tropical cyclone waves from satellite altimetry observations, Advances in Space Research, https://doi.org/10.1016/j.asr.2019.07.021

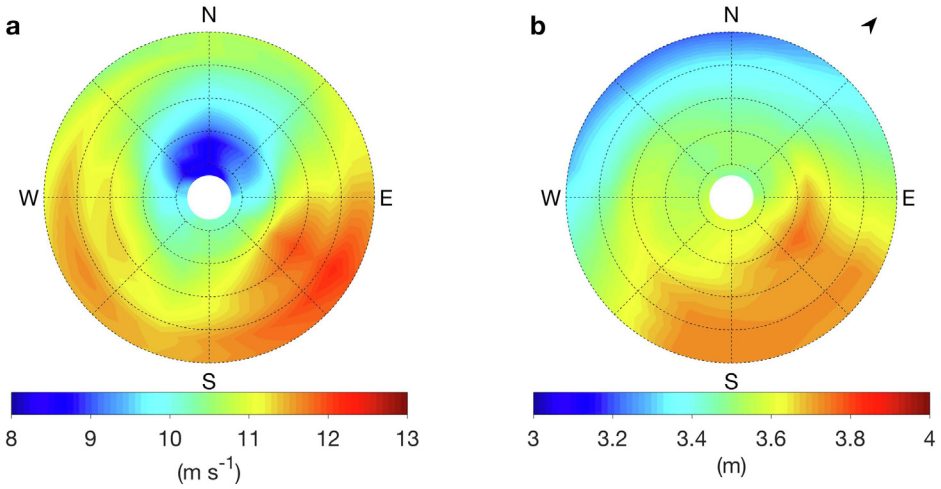

Fig. 6. Altimeter derived composites of (a) 10 – m wind speed and (b) significant wave height for the 1998–2012 period.

Rudeva and Gulev (2010) that locates the NCEP/NCAR reanalysis composite cyclone's maximum wind speed in the Southeast sector with maximum values of the order of 10 m/s. In the composite analysis of ERA-40 and global circulation model (GCM) winter cyclones of Bauer and Del Genio (2006), the maximum wind speed at 850 hPa, with values of 19 m/s (GCM) and 23 m/s (ERA-40) also appears in the southeast sector, roughly at the edge of a 5° box around at the cyclone's center. A secondary zone of high winds appears in the southwest quadrant, with lower maxima.

The distribution of high winds agrees with the warm/-cold conveyor belt (W/CCB) model (Semple, 2006) of extra-tropical cyclones. The WCB, that extends along the cold front and is associated with strong sustained winds in the Southeast quadrant, appears earlier than the CCB in the cyclone's life cycle, while this last feature is associated with strong winds in the western part of the cyclone, as the CCB wraps around the center cyclonically (Hewson and Neu, 2015).

The Hs composite map (Fig. 6b) for the same period was obtained by averaging the annual maps. The highest average Hs is 3.768 m, located on azimuth 120° and 194 km from the cyclone center. The high Hs (>3.6 m) region extends from azimuth 113° to 207° and from 166 km from the center, covering almost the whole SE quadrant and part of the SW quadrant.

Higher Hs have been found in that location either in analysis of single cyclones (Ponce de León and Guedes Soares, 2014) or in the composite analysis of Kita et al. (2018), that looked at explosive cyclones only, while we included both non-explosive and explosive cyclones in our census. The mechanism responsible for this structure of the Hs field is the *extended fetch* mechanism: ocean waves to the right of the center of cyclones evolve under a running fetch condition so waves generated there propagate in cyclone's direction, experiencing strong winds for a longer duration than other areas under the cyclone. The waves remain in this region of extended fetch and propagate approximately in the wind's direction, resulting in higher Hs than in other regions (Kita et al., 2018; Young and Vinoth, 2013). Following this hypothesis, the strong northerly winds in the western section of the cyclone (Field and Wood, 2007) do not have a corresponding high Hs area, since these winds are not aligned with the cyclone's propagation direction (largely eastward).

3.2. Hs composites during the cyclone life cycle

The cyclone life cycle was divided in three stages: development, maximum strength and decay (Dacre et al., 2012). The development stage goes from cyclogenesis to 24 h before the SLP minimum and is characterized by the appearance of the warm sector between the cold and warm fronts, the development of a closed cyclonic circulation, a drop in central SLP and the increase of system-relative wind speeds; the maximum strength stage encompasses the 48 h interval around the SLP minimum, when the lowest central pressure occurs and the large pressure gradient produces peak wind speeds; the decay stage goes from 24 h after the SLP minimum to cyclone lysis, during which the SLP minimum increases and pressure gradients decrease, leading to lower wind speeds and the warm front wraps around the cyclone center, forming the CCB. The life cycle stages are defined with respect to the time of SLP minimum and so are independent of the actual length of life of individual cyclones.

The Hs composites (Fig. 7) show a marked difference between life cycle stages from the development stage ($2.7\ m < Hs < 3.3\ m$), through the maximum strength stage ($3.7\ m < Hs < 4.6\ m$) to the decay stage ($3.2\ m < Hs < 3.6\ m$). In the development stage (Fig. 7a), the Hs is higher east and south of the center, consistent with the development of the cyclonic circulation and the appearance of the WCB in the warm sector of the cyclone (Dacre and Gray, 2009; Hewson and Neu, 2015). During

Please cite this article as: S. Ponce de León and J. H. Bettencourt, Composite analysis of North Atlantic extra-tropical cyclone waves from satellite altimetry observations, Advances in Space Research, https://doi.org/10.1016/j.asr.2019.07.021

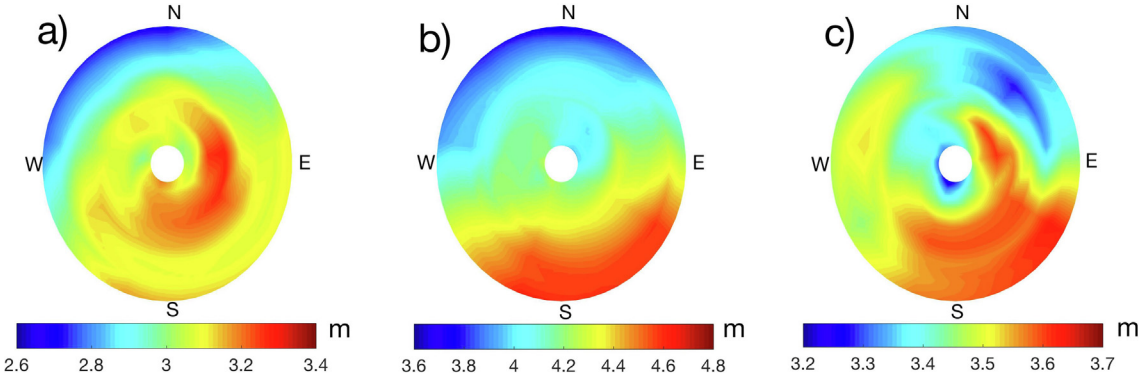

Fig. 7. Hs composite in the cyclone life cycle stages. (a) Development stage: up to 24 h before SLP minimum; (b) Maximum strength stage: from 24 h before to 24 h after SLP min; (c) Decay stage; from 24 h after SLP minimum to cyclone lysis. Note the different colour bar scales for each panel.

the maximum strength stage (Fig. 7b), the Hs reaches the maximum values in the south sector as the extended fetch mechanism comes in to play. In the decay stage (Fig. 7c), we observe the appearance of a high Hs region in the Northwest sector of the cyclone that could be the signature of the CCB as the fronts wrap cyclonically around the cyclone's center and produces strong winds in this region (zone B in Kita et al. (2018)).

3.3. Hs composites for different cyclone intensities

The cyclones were divided in five intensity classes, measured by how much the cyclone deepens during its lifetime, using the difference between the center's SLP minimum and the center's SLP at cyclogenesis (DSLP).

In our cyclone census DSLP does not show a strong dependence on cyclone lifetime, as the average cyclone duration is similar in every quintile (~5 days), however we find that the percentage of short-lived cyclones (4 to 6 days) is the highest (>50%) in the 5th quintile.

As the cyclone intensity increases, the Hs increases, and we observe a shift of the high Hs region from the western to the eastern half of the cyclone. Cyclones in the 1st and 2nd quintiles show a similar Hs composite structure (Fig. 8 a, b) with higher wave heights in the southwest quadrant. In the 3rd quintile (Fig. 8c), a region of high Hs appears in the southeast quadrant near the 90° azimuth, extending to the complete quadrant in the 4th quintile (Fig. 8d). In the 5th quintile (Fig. 8e), large Hs is observed in the eastern half of the cyclone.

This behaviour of the Hs composite is due not only to the increase in wind speed with cyclone intensity, which occurs on both west and east halves (Rudeva and Gulev, 2010), but also to the differences in the evolution of weak and strong cyclones. Strong cyclones move more meridionally than weaker cyclones (Sanders, 1986) thus the eastern half will have the wind, blowing cyclonically towards the North, better aligned with the propagation direction of the cyclone. In our census, the cyclones of the 5th quintile move, on average, in the 32.6° direction (measured from North), while the weaker cyclones (1st quintile) move in the 48.4° direction; therefore, the extended fetch mechanism will act in the eastern half of the cyclone for the stronger cyclones.

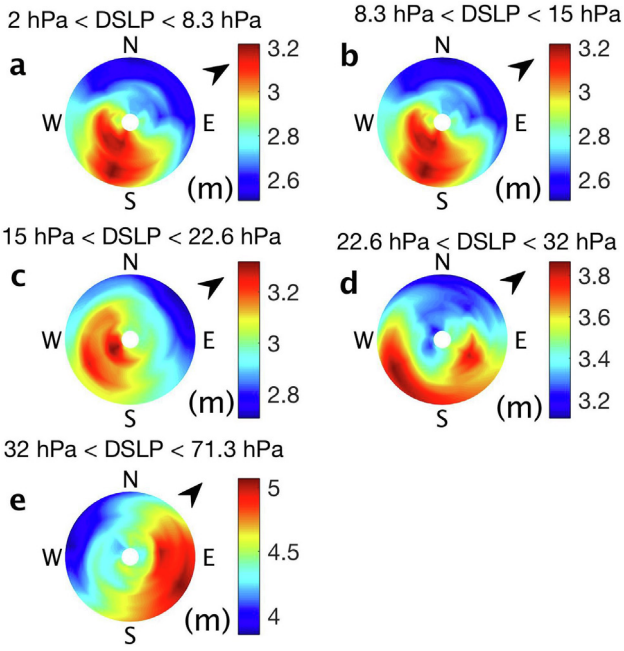

Fig. 8. Hs composites by cyclone intensity class. DSLP is the difference between the centre's SLP minimum and the centre's SLP at cyclogenesis. Note the different colour bar scales.

3.4. Distributions of cyclone significant wave height

The composite analysis of the previous sections gave a general view of the organization of the Hs field of extra-tropical cyclones and how it depends on cyclone strength and life cycle stage. Here, we study the magnitude of Hs in cyclones with respect to basin scale values of Hs. Specifically, we computed probability density functions (*pdf*) of Hs using the altimeter derived Hs measurements for the North Atlantic basin above 15°N and for those measurements whose distance to the cyclone centers was less than R.

Please cite this article as: S. Ponce de León and J. H. Bettencourt, Composite analysis of North Atlantic extra-tropical cyclone waves from satellite altimetry observations, Advances in Space Research, https://doi.org/10.1016/j.asr.2019.07.021

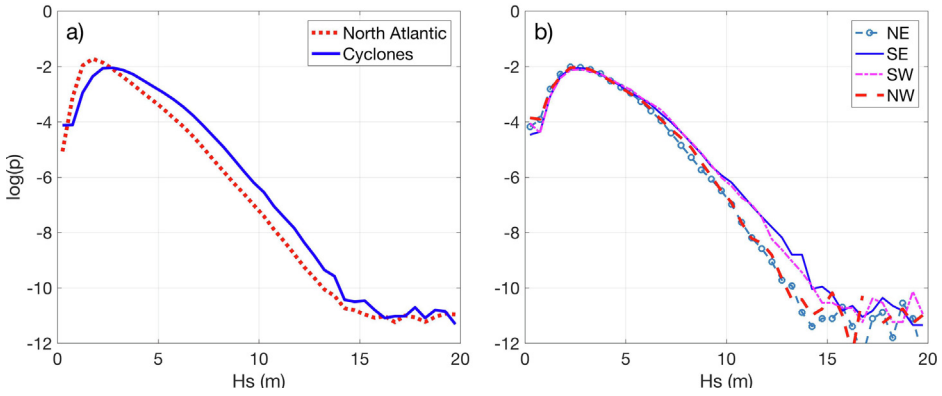

Fig. 9. Normalized probability density function of significant wave height. (a) North Atlantic basin and cyclones; (b) by quadrant.

Although the Hs composite values of Fig. 6b are below the high Hs that are usually associated with individual cyclones, the distribution of cyclone Hs (Fig. 9a), clearly shows that the Hs in cyclones is likely to be higher than that for the North Atlantic. Inside the cyclone, the Hs *pdfs* by quadrant (Fig. 9b) show a higher probability of large Hs in the southern part of the cyclone. This is consistent with the average picture given by the composite analysis.

The sample L-moments (Hosking, 1990) of the Hs distributions (Table 1) show that the mean Hs increases 0.87 m from the North Atlantic data to the cyclone data set (the right shift of the *pdf* plots in Fig. 9a). The second L-moment λ_2, that measures the characteristic dispersion of the data, is only slightly higher for the cyclones. Both the skewness and kurtosis ($\tau_{3,4} = \lambda_{3,4}/\lambda_2$) are lower for the cyclone Hs data. This means that the *pdf* of the Hs in cyclones is less skewed and broader than the *pdf* of the Hs in the North Atlantic therefore favouring larger Hs (Hanafin et al., 2012) in the regions under the influence of the cyclones.

The differences in the Hs *pdf* inside the cyclone region are found essentially in the Hs > 10 m region (Fig. 9b), where the southern quadrants have larger probabilities than the northern quadrants. The mean Hs differences between the south and north parts of the cyclone are of 25 cm, with the former having slightly higher dispersion. In terms of the 3rd and 4th L-moments, the quadrant's Hs *pdf* have lower τ_3 and larger τ_4 than the whole cyclone *pdf*.

The lower skewness means that quadrant *pdfs* are more symmetric than the cyclone *pdf*, although the difference between the cyclone and the SE quadrant is very small. The lower kurtosis of the quadrant *pdfs* with respect to the cyclone kurtosis means broader distributions for the individual quadrants, although less so for the SE quadrant.

Table 1
L – moments of the Hs distributions. North Atlantic: North Atlantic basin above 15°N; Cyclones: data measured less than 500 km from the cyclone centres; NE Quadrant: cyclone data measured between 0° and 90° from North; SE Quadrant: cyclone data measured between 90° and 180° from North; SW Quadrant: cyclone data measured between 180° and 270° from North; NW Quadrant: cyclone data measured between 270° and 0° from North.

	Mean (λ_1)	Dispersion (λ_2)	Skewness (τ_3)	Kurtosis (τ_4)
North Atlantic	2.77 m	0.88 m	0.191	0.196
Cyclones	3.64 m	1 m	0.157	0.152
NE Quadrant	3.42 m	0.96 m	0.135	0.157
SE Quadrant	3.67 m	1.05 m	0.155	0.169
SW Quadrant	3.71 m	1.07 m	0.133	0.161
NW Quadrant	3.46 m	1 m	0.134	0.162

4. Discussion and conclusions

The composite analysis performed on the Hs maps, obtained from 15 years of satellite altimetry measurements, highlighted common features of the Hs distribution under extra-tropical cyclones in the North Atlantic. The main feature of this distribution (Fig. 6b) is the maximum in the SE quadrant of the composite cyclone, due to the extended fetch mechanism. This finding agrees with the results of Kita et al. (2018) that used composites of hindcasted significant wave height in the NW Pacific to reach the same conclusion. Since compositing eliminates details of individual events, it is natural to assume that the composite Hs distribution of Fig. 6b is subject to a large degree of variability. Indeed, when looking at specific positions of the composite maps, we found standard deviations in Hs that can reach 80% of the composite Hs (not shown). Such large variability has been noted in composite studies before (Rudeva and Gulev, 2010) and is a consequence of the great variety of cyclone characteristics that make part of the cyclone census.

The change in cyclone characteristics during their lifetime prompted us to look at Hs composites in different phases of the lifetime of cyclones. Unlike Kita et al. (2018), that used the cyclone's propagation direction as the reference direction in the composite mapping procedure and Young and Vinoth (2013) that accounted for the storm direction to understand the radial structure of tropical cyclones, which have a axisymmetric wind field, we use a fixed orientation (North, $\alpha = 0°$) thus our composites of

Please cite this article as: S. Ponce de León and J. H. Bettencourt, Composite analysis of North Atlantic extra-tropical cyclone waves from satellite altimetry observations, Advances in Space Research, https://doi.org/10.1016/j.asr.2019.07.021

Fig. 7, show also the effect of the propagation direction of the cyclone in the Hs composite distribution as this factor combines with the changes in the cyclone's wind system to influence the extended fetch mechanism.

In Kita et al. 2018, the maximum in composite Hs was found 12 h after the maximum strength time, which is consistent with our analysis that finds the Hs maximum within 48 h of the maximum strength time.

The difference between maximum composite Hs between the weakest and strongest cyclones is approximately 2 m which is the same magnitude of the difference of the climatological Hs between the extra-tropical and tropical North Atlantic (Gulev et al., 1998; Sterl and Caires, 2006). Stronger cyclones, that track a more northerly path, have maximum composite Hs in the eastern half, which is again consistent with the extended fetch mechanism, since this is the part of the cyclone that will have winds blowing in the same direction of the cyclone's propagation.

It was already reported by Young (1999), that the maximum Hs in the Northern Hemisphere occur in the North Atlantic (maximum mean monthly value of Hs = 5.2 m) and that the seasonal variability in the Northern Hemisphere is much greater than in the Southern Hemisphere. Probability density functions of Hs show that in the cyclone region, Hs between 3 and 15 m are more probable than in the whole North Atlantic basin above 15° N. Linear order statistics (L-moments) show that the *pdf* for the cyclone is less skewed and broader than the *pdf* for the basin. The higher value of τ_4 for the SE quadrant implies a narrower Hs *pdf*, which could be interpreted as a stronger tendency for higher waves in this quadrant, a result of the general cyclonic wind pattern and trajectory of the cyclone ensemble that was studied in this paper, independently of the individual variability of the cyclone census.

The maximum track density (Fig. 5b) is collocated with the extreme Hs region of Takbash et al. (2018), which signals the dominant role of extratropical storms in setting the wave climate in the North Atlantic. In this region, wind-sea dominates and the correlation between daily averaged wind speed and wave height is strong (Stopa et al., 2013). The correlation diminishes in the eastern boundary of the basin, were the longest waves in the Atlantic Ocean occur (Young, 1999), signalling the transition from a wind sea dominated wave climate to one dominated by swell that propagates away from the storm track region.

In the present climate, a shift of extratropical storms to higher latitudes has been identified (Trigo, 2006; Wang et al., 2006), related to a strong positive correlation with the Artic Oscillation Index (Stopa et al., 2013). This northward shift is expected to continue in global warming scenarios for strong cyclones (Pinto et al., 2006). North Atlantic storms future climate studies appear to show a decrease in extratropical cyclones for 2xCO2 experiments in most of the North Atlantic, except in the North Sea and Bay of Biscay (Beersma et al., 1997; WASA, 1998), a trend which is confirmed in more recent studies, but with increasing winter storm intensity (Ulbrich et al., 2009). Relating these findings and projections to changes in the structure of the Hs field under cyclones is not straightforward because we could not find data on the future projected changes of the characteristic airflows of the cyclones. We can expect that an increase in the winter intensity of cyclones may lead to an increase in the Hs and some evidence of increased zonal propagation of intense cyclones (Raible and Blender, 2004) may indicate a shift in the position of the maximum Hs.

We used 15 years of satellite altimetry to perform this study. This is approximately half of the total period of available radar altimetry measurements of wind and significant wave height. We plan to extend the database to the full period and report back on the results. Another topic of future work is to combine the extra-tropical cyclone information with tropical cyclone census to perform a similar study for the latter (see Young and Vinoth (2013)) and compare the characteristics of the significant wave height composites.

Acknowledgements

The authors acknowledge the GLOBWAVE project team for their assistance with the data retrieval process. SPL acknowledges the European Space Agency for the travel support to attend the 25 Years of Progress in Radar Altimetry (25YPRA), in Azores. We acknowledge Dr. Jerome Benveniste for bringing to our attention the ESA Atlantic from Space workshop.

References

Abdalla, S., Janssen, P.A.E.M., Bidlot, J.-R., 2010. Jason-2 OGDR wind and wave products: monitoring, validation and assimilation. Mar. Geod. 33, 239–255. https://doi.org/10.1080/01490419.2010.487798.

Alves, J.H., Young, I.R., 2003. On estimating extreme wave heights using combined Geosat, Topex/Poseidon and ERS-1 altimeter data. Appl. Ocean Res. 25, 167–186. https://doi.org/10.1016/j.apor.2004.01.002.

Ash, E., Carter, D., Collard, F., Busswell, G., 2010. Satellite Wave Data Quality Report (No. GlobWave/DD/SWDQR). SatOC. https://projets.ifremer.fr/content/download/5120/37286/GlobWave_D.16_SWDQR.pdf

Bauer, M., Del Genio, A.D., 2006. Composite analysis of winter cyclones in a GCM: influence on climatological humidity. J. Clim. 19, 1652–1672. https://doi.org/10.1175/JCLI3690.1.

Beersma, J.J., Rider, K.M., Komen, G.J., Kaas, E., Kharin, V.V., 1997. An analysis of extra-tropical storms in the North Atlantic region as simulated in a control and 2 × CO2 time-slice experiment with a high-resolution atmospheric model. Tellus A 49, 347–361. https://doi.org/10.1034/j.1600-0870.1997.t01-2-00003.x.

Bell, R.J., Gray, S.L., Jones, O.P., 2017. North Atlantic storm driving of extreme wave heights in the North Sea. J. Geophys. Res. Oceans 122, 3253–3268. https://doi.org/10.1002/2016JC012501.

Breivik, Ø., Aarnes, O.J., Abdalla, S., Bidlot, J.-R., Janssen, P.A.E.M., 2014. Wind and wave extremes over the world oceans from very large ensembles. Geophys. Res. Lett. 41, 5122–5131. https://doi.org/10.1002/2014GL060997.

Chang, E.K.M., Song, S., 2006. The seasonal cycles in the distribution of precipitation around cyclones in the Western North Pacific and Atlantic. J. Atmospheric Sci. 63, 815–839. https://doi.org/10.1175/JAS3661.1.

Dacre, H.F., Gray, S.L., 2009. The spatial distribution and evolution characteristics of North Atlantic cyclones. Mon. Weather Rev. 137, 99–115. https://doi.org/10.1175/2008MWR2491.1.

Dacre, H.F., Hawcroft, M.K., Stringer, M.A., Hodges, K.I., 2012. An extratropical cyclone atlas: a tool for illustrating cyclone structure and evolution characteristics. Bull. Am. Meteorol. Soc. 93, 1497–1502. https://doi.org/10.1175/BAMS-D-11-00164.1.

Field, P.R., Wood, R., 2007. Precipitation and cloud structure in midlatitude cyclones. J. Clim. 20, 233–254. https://doi.org/10.1175/JCLI3998.1.

Giordani, H., Caniaux, G., 2001. Sensitivity of cyclogenesis to sea surface temperature in the Northwestern Atlantic. Mon. Weather Rev. 129, 1273–1295. https://doi.org/10.1175/1520-0493(2001) 129<1273:SOCTSS>2.0.CO;2.

Graham, N.E., Diaz, H.F., 2001. Evidence for intensification of North Pacific winter cyclones since 1948. Bull. Am. Meteorol. Soc. 82 (9), 1869–1893.

Gramcianinov, C.B., Hodges, K.I., Camargo, R., 2019. The properties and genesis environments of South Atlantic cyclones. Clim. Dyn. https://doi.org/10.1007/s00382-019-04778-1.

Gulev, S.K., Cotton, D., Sterl, A., 1998. Intercomparison of the North Atlantic wave climatology from voluntary observing ships, satellite data and modelling. Phys. Chem. Earth 23, 587–592. https://doi.org/10.1016/S0079-1946(98)00075-5.

Hewson, T.D., 2009. Diminutive frontal waves—a link between fronts and cyclones. J. Atmospheric Sci. 66, 116–132. https://doi.org/10.1175/2008JAS2719.1.

Hewson, T.D., Neu, U., 2015. Cyclones, windstorms and the IMILAST project. Tellus Dyn. Meteorol. Oceanogr. 67, 27128. https://doi.org/10.3402/tellusa.v67.27128.

Hosking, J.R.M., 1990. L-Moments: Analysis and estimation of distributions using linear combinations of order statistics. J. R. Stat. Soc. Ser. B Methodol. 52, 105–124. https://doi.org/10.1111/j.2517-6161.1990.tb01775.x.

Hoskins, B.J., Valdes, P.J., 1989. On the existence of storm-tracks. J. Atmospheric Sci. 47, 1854–1864. https://doi.org/10.1175/1520-0469(1990) 047<1854:OTEOST>2.0.CO;2.

Hurrell, J.W., van Loon, H., 1997. Decadal variations in climate associated with the North Atlantic oscillation. Clim. Change 36, 301–326. https://doi.org/10.1023/A:1005314315270.

Izaguirre, C., Méndez, F.J., Menéndez, M., Losada, I.J., 2011. Global extreme wave height variability based on satellite data. Geophys. Res. Lett. 38, L10607, https://doi.org/10.1029/2011GL047302.

Janssen, P.A.E.M., Abdalla, S., Hersbach, H., Bidlot, J.-R., 2007. Error estimation of buoy, satellite, and model wave height data. J. Atmospheric Ocean. Technol. 24, 1665–1677. https://doi.org/10.1175/JTECH2069.1.

Kita, Y., Waseda, T., Webb, A., 2018. Development of waves under explosive cyclones in the Northwestern Pacific. Ocean Dyn. 68, 1403–1418. https://doi.org/10.1007/s10236-018-1195-z.

Lozano, I., Devoy, R.J.N., May, W., Andersen, U., 2004. Storminess and vulnerability along the Atlantic coastlines of Europe: analysis of storm records and of a greenhouse gases induced climate scenario. Mar. Geol. 210, 205–225. https://doi.org/10.1016/j.margeo.2004.05.026.

Martin, S., 2014. An Introduction to Ocean Remote Sensing, second ed. Cambridge University Press, New York.

Pinto, J.G., Gómara, I., Masato, G., Dacre, H.F., Woollings, T., Caballero, R., 2014. Large-scale dynamics associated with clustering of extratropical cyclones affecting Western Europe. J. Geophys. Res. Atmospheres 119, 13704–13719. https://doi.org/10.1002/2014JD022305.

Pinto, J.G., Spangehl, T., Ulbrich, U., Speth, P., 2006. Assessment of winter cyclone activity in a transient ECHAM4-OPYC3 GHG experiment [WWW Document]. https://www.ingentaconnect.com/content/schweiz/mz/2006/00000015/00000003/art00004.

Ponce de León, S., Guedes Soares, C., 2014. Extreme wave parameters under North Atlantic extratropical cyclones. Ocean Model. 81, 78–88. https://doi.org/10.1016/j.ocemod.2014.07.005.

Ponce de Leon, S., Bettencourt, J.H., Brennan, J., Dias, F., 2015. Evolution of the extreme wave region in the North Atlantic using a 23 year Hindcast p. V003T02A019-V003T02A019. Presented at the ASME 2015 34th International Conference on Ocean, Offshore and Arctic Engineering. American Society of Mechanical Engineers.

Ponce de León, S., Guedes Soares, C., 2015. Hindcast of extreme sea states in North Atlantic extratropical storms. Ocean Dyn. 65 (2), 241–254. https://doi.org/10.1007/s10236-014-0794-6.

Queffelou, P., 2004. Long-Term validation of wave height measurements from Altimeters. Mar. Geod. 27, 495–510. https://doi.org/10.1080/01490410490883478.

Raible, C.C., Blender, R., 2004. Northern Hemisphere midlatitude cyclone variability in GCM simulations with different ocean representations. Clim. Dyn. 22, 239–248. https://doi.org/10.1007/s00382-003-0380-y.

Rudeva, I., Gulev, S.K., 2010. Composite analysis of North Atlantic extratropical cyclones in NCEP–NCAR reanalysis data. Mon. Weather Rev. 139, 1419–1446. https://doi.org/10.1175/2010MWR3294.1.

Sanders, F., 1986. Explosive cyclogenesis in the West-Central North Atlantic Ocean, 1981–84. Part I: composite structure and mean behavior. Mon. Weather Rev. 114, 1781–1794. https://doi.org/10.1175/1520-0493(1986) 114<1781:ECITWC>2.0.CO;2.

Sanders, F., Gyakum, J.R., 1980. Synoptic-dynamic climatology of the "Bomb". Mon. Weather Rev. 108, 1589–1606. https://doi.org/10.1175/1520-0493(1980) 108<1589:SDCOT>2.0.CO;2.

Schneidereit, A., Blender, R., Fraedrich, K., 2010. A radius –depth model for midlatitude cyclones in reanalysis data and simulations. Q. J. R. Meteorol. Soc. 136, 50–60. https://doi.org/10.1002/qj.523.

Semple, A.T., 2006. A review and unification of conceptual models of cyclogenesis. Meteorol. Appl. 10, 39–59. https://doi.org/10.1017/S135048270300505X.

Serreze, M.C., 2009. Northern Hemisphere Cyclone Locations and Characteristics from NCEP/NCAR Reanalysis Data, Version 1.

Serreze, M.C., Carse, F., Barry, R.G., Rogers, J.C., 1997. Icelandic low cyclone activity: climatological features, linkages with the NAO, and relationships with recent changes in the northern hemisphere circulation. J. Clim. 10, 453–464. https://doi.org/10.1175/1520-0442(1997)010<0453:ILCACF>2.0.CO;2.

Sterl, A., Caires, S., 2006. Climatology, variability and extrema of ocean waves: the web-based KNMI/ERA-40 Wave Atlas. In: Volume 3: Safety and Reliability; Materials Technology; Douglas Faulkner Symposium on Reliability and Ultimate Strength of Marine Structures. Presented at the 25th International Conference on Offshore Mechanics and Arctic Engineering, pp. 833–842.

Stopa, J.E., Cheung, K.F., Tolman, H.L., Chawla, A., 2013. Patterns and cycles in the Climate Forecast System Reanalysis wind and wave data. Ocean Model. 70, 207–220. https://doi.org/10.1016/j.ocemod.2012.10.005.

Takbash, A., Young, I.R., Breivik, Ø., 2018. Global wind speed and wave height extremes derived from long-duration satellite records. J. Clim. 32, 109–126. https://doi.org/10.1175/JCLI-D-18-0520.1.

Trenberth, K.E., Hurrell, J.W., 1994. Decadal atmosphere-ocean variations in the Pacific. Climate Dyn. 9, 303–319. https://doi.org/10.1007/BF00204745.

Trigo, I.F., 2006. Climatology and interannual variability of storm-tracks in the Euro-Atlantic sector: a comparison between ERA-40 and NCEP/NCAR reanalyses. Clim. Dyn. 26, 127–143. https://doi.org/10.1007/s00382-005-0065-9.

Ulbrich, U., Leckebusch, G.C., Pinto, J.G., 2009. Extra-tropical cyclones in the present and future climate: a review. Theor. Appl. Climatol. 96, 117–131. https://doi.org/10.1007/s00704-008-0083-8.

Wang, X.L., Swail, V.R., 2002. Trends of atlantic wave extremes as simulated in a 40-Yr wave Hindcast using kinematically reanalyzed wind fields. J. Clim. 15, 1020–1035. https://doi.org/10.1175/1520-0442(2002) 015<1020:TOAWEA>2.0.CO;2.

Wang, X.L., Swail, V.R., Zwiers, F.W., 2006. Climatology and changes of extratropical cyclone activity: comparison of ERA-40 with NCEP–

Please cite this article as: S. Ponce de León and J. H. Bettencourt, Composite analysis of North Atlantic extra-tropical cyclone waves from satellite altimetry observations, Advances in Space Research, https://doi.org/10.1016/j.asr.2019.07.021

NCAR reanalysis for 1958–2001. J. Clim. 19, 3145–3166. https://doi.org/10.1175/JCLI3781.1.

WASA, 1998. Changing waves and storms in the Northeast Atlantic? Bull. Am. Meteorol. Soc. 79, 741–760. https://doi.org/10.1175/1520-0477(1998) 079<0741:CWASIT>2.0.CO;2.

Young, I.R., 1999. Seasonal variability of the global ocean wind and wave climate. Int. J. Climatol. 19, 931–950. https://doi.org/10.1002/(SICI)1097-0088(199907)19:9<931::AID-JOC412>3.0.CO;2-O.

Young, I.R., Vinoth, J., 2013. An "extended fetch" model for the spatial distribution of tropical cyclone wind–waves as observed by altimeter. Ocean Eng. 70, 14–24. https://doi.org/10.1016/j.oceaneng.2013.05.015.

Young, I.R., Sanina, E., Babanin, A.V., 2017. Calibration and cross-validation of a global wind and wave database of Altimeter, Radiometer and Scatterometer measurements. J. Atmos. Oceanic Technol. 34, 1285–1306. https://doi.org/10.1175/JTECH-D-16-0145.1.

Young, I.R., Donelan, M.A., 2018. On the determination of global ocean wind and wave climate from satellite observations. Remote Sens. Environ. 215, 228–241. https://doi.org/10.1016/j.rse.2018.06.006.

Zieger, S., Vinoth, J., Young, I.R., 2009. Joint calibration of multiplatform altimeter measurements of wind speed and wave height over the Past 20 Years. J. Atmospheric Ocean. Technol. 26, 2549–2564. https://doi.org/10.1175/2009JTECHA1303.1.

Please cite this article as: S. Ponce de León and J. H. Bettencourt, Composite analysis of North Atlantic extra-tropical cyclone waves from satellite altimetry observations, Advances in Space Research, https://doi.org/10.1016/j.asr.2019.07.021